

3D Helical Micromixer Fabricated by Micro Lost-Wax Casting

Daiki Tachibana, Ken Matsubara, Ryosuke Matsuda, Taichi Furukawa, Shoji Maruo, Yoshimi Tanaka, Ohmi Fuchiwaki,* and Hiroki Ota*

Micromixers produced by micro fabrication techniques have attracted attention for micro total analysis systems and lab-on-a-chip applications in point-of-care testing. However, the fabrication and setup of micromixers have become more complex and more difficult. Considering the practical use of micromixers in medical and industrial applications, their designs can be simplified while maintaining high mixing efficiency. Rapid prototyping, represented by 3D printing having micro-scale resolutions, is one promising technology to replace conventional fabrication methods such as soft lithography. Here, a 3D helical micromixer fabricated by micro-scale lost-wax casting is reported. The molds for lost-wax casting are fabricated by fine 3D printing of a hard wax resin which can be removed from a polydimethylsiloxane block just by heating and washing with water, and a fine and smooth structure is realized. The optimized helical micromixer fabricated by lost-wax casting promotes mixing efficiency compared with other micromixers. In addition, a monolithic microchannel having the helical 3D bridge structure is presented in this study. The demonstration is an important advancement toward the industrial applications of micromixers fabricated by micro-scale 3D printing. The ability to fabricate complex structures can simply lead to the creation of more sophisticated mixers in the future.

Many micro total analysis systems (microTAS) and lab-on-a-chip applications have been developed that provide various functions such as mixing,^[1,2] heating,^[3,4] separation,^[5–7] and extraction.^[8,9] These applications are crucial to point-of-care testing (POCT), especially in developing countries.^[10] These

D. Tachibana, K. Matsubara, R. Matsuda, Prof. T. Furukawa, Prof. S. Maruo, Prof. O. Fuchiwaki, Prof. H. Ota
Department of Mechanical Engineering
Yokohama National University
79-5 Tokiwadai, Hodogaya-ku, Yokohama 240-8501, Japan
E-mail: fuchiwaki-ohmi-xk@ynu.ac.jp; ota-hiroki-xm@ynu.ac.jp
Prof. T. Furukawa, Prof. S. Maruo, Prof. O. Fuchiwaki, Prof. H. Ota
Graduate School of System Integration
Yokohama National University
79-5 Tokiwadai, Hodogaya-ku, Yokohama 240-8501, Japan
Y. Tanaka
Graduate School of Environment and Information Science
Yokohama National University
79-5 Tokiwadai, Hodogaya-ku, Yokohama 240-8501, Japan

 The ORCID identification number(s) for the author(s) of this article can be found under <https://doi.org/10.1002/admt.201900794>.

DOI: 10.1002/admt.201900794

microTAS applications use straight channels, which require a long distance until mixing is completed and leads the system to become larger. Various structures and external components for promoting mixing have been developed, including an external actuator^[11] and a large mixing channel composed of multiple microchannels having a short diffusion distance.^[12] There is also a wave-shaped micromixer whose diameter is changed for an arbitrary period to promote chaotic advection.^[13–15] However, these micromixers complicate the channel structure and fabrication process, making the latter more difficult.^[16] Moreover, it is difficult to fabricate these complicated structures with “high accuracy,” including a 3D structure. Therefore, there is a high demand for micromixers, which have a high mixing function with a simple system and a simple fabrication process.

Regarding fabrication methods of microTAS that include micromixers, soft lithography has been the main device fabrication method.^[17–21] Soft lithography, however, requires various specific fabrication facilities. The fabrication process is 2D and consists of three main steps: chemical fabricating of molds, molding, and bonding of substrate materials.^[22] To construct a 3D structure, additional steps are required.^[23,24] A few fabrication methods using 3D-printed microchannels have been developed.^[25–29] These methods have one printing step for making molds, and can make a 3D structure without the bonding step.^[30] These fabrications use sacrificial molds, e.g., acrylonitrile butadiene styrene (ABS) resin, silica, and polyvinyl alcohol (PVA).^[31–33] However, these methods cannot easily make fine 3D structures with dimensions less than 100 μm , because the mold fabrications by 3D printing are based on fused deposition modeling (FDM)-type 3D printings. Additionally, they require hazardous solutions such as acetone^[34] or hydrogen fluoride^[35] to remove 3D-printed microchannel mold from the polydimethylsiloxane (PDMS) block. Recently, microfluidic devices are also used for wearable devices.^[36–38] It might be better not to use as few harmful chemicals as possible. In terms of a PVA mold, PVA can easily be removed with water.^[31] However, it absorbs the water in the air (moisture), and can deform the shape easily, which leads to increasing

the error in the fabrication process. In addition, ABS and PVA require several hours or days until they are completely removed.^[39] There is also a method of making microfluidic devices with 3D printers. It consumes a lot of 3D printer resin and costs more to use a high-precision 3D printer. Flexible

resin for 3D printing is not transparent like PDMS, which makes observation of the inside difficult.

Here, we propose a micromixer with a 3D screw-like helical structure with high mixing efficiency fabricated by a lost-wax casting (Figure 1a,b). Helical microchannels with

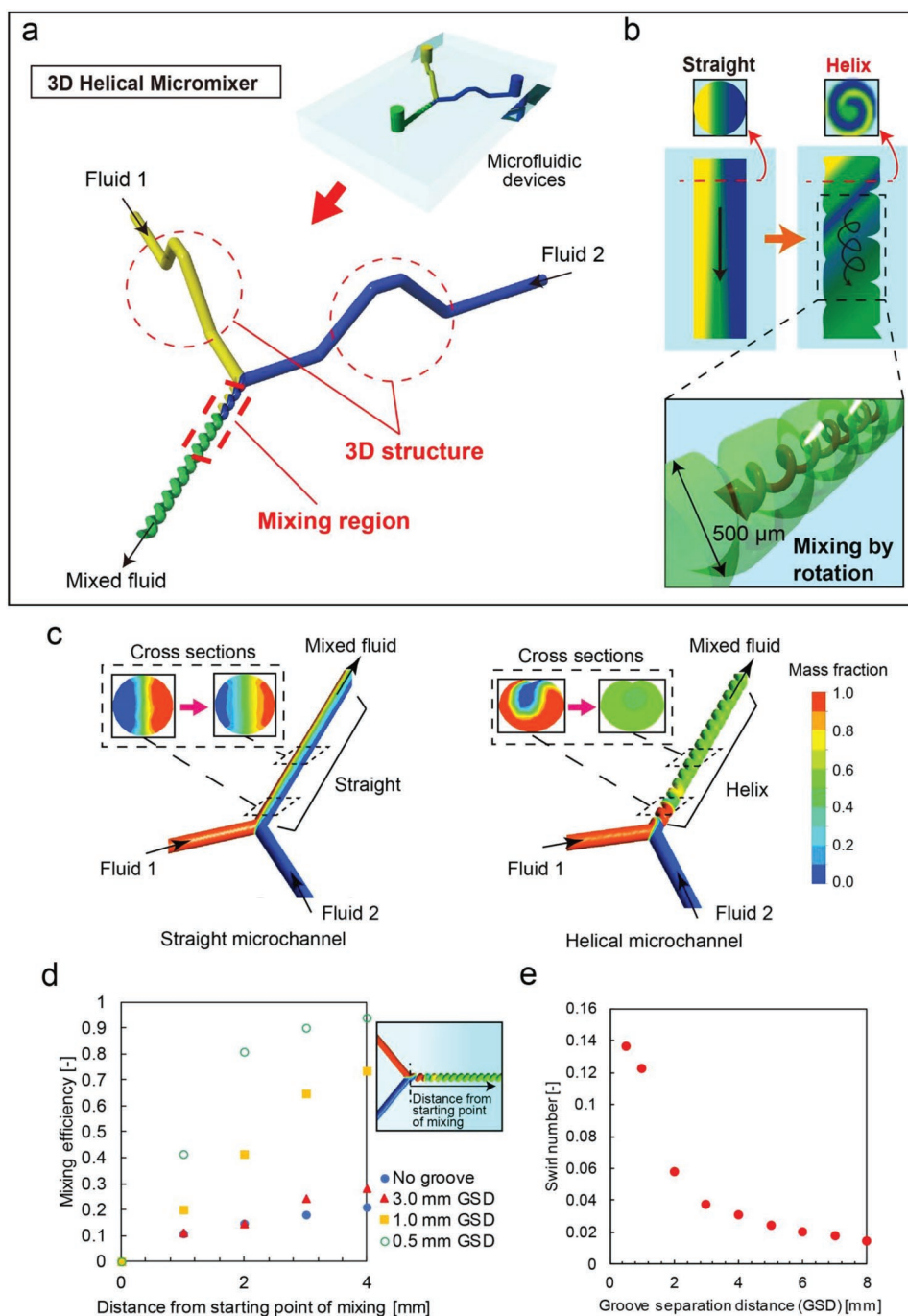


Figure 1. Schematic drawings and simulation results of a 3D helical micromixer. a) Monolithic microchannel composed of the helical micromixer and 3D structure. b) In the straight microchannel, the two fluids, yellow and blue inks, mixed gradually by diffusion. In the 3D helical micromixer, the two fluids rotated and generated secondary flow according to the helical structure inside the microchannel, which promoted the mixing efficiency. c) CFD simulations of fluid flows in straight and helical microchannels. Red and blue indicate two different fluids which became a green mixture on mixing. d) Relationship between the distance from the starting point of mixing and the mixing efficiency. Mixing efficiency based on variance of mass fraction became higher with respect to smaller GSD. e) Relationship between GSD inside the micromixer and swirl number. The swirl number monotonically decreases with respect to larger GSD.

micro triangular grooves generate a secondary flow inside the channels. This secondary flow causes the two fluids to pass through the channel with rotation. During the secondary flow, the contact area of the two fluids increases, and advection of the liquids takes place. Eventually, the mixing efficiency of the fluids in the helical microchannel is promoted. A mold to make microchannels within the device is made by a single-step fabrication process based on inkjet-type high-resolution 3D printing with wax resin. Removal of the wax-resin from a substrate is done using water; no hazardous chemicals are necessary, and the wax mold can reliably be removed within an hour after heated. Our fabrication process, which is based on sacrificial molds, saves on fabrication time.

In order to investigate the mixing efficiency, we simulated movement of the mass fraction by computational fluid dynamics (CFD) analysis. Figure 1c shows the simulated mixing of two fluids inside the straight and helical microchannels. Red and blue colors represent mass fractions of fluids 1 and 2, respectively. In the green area, the mass fraction of fluid 1 or 2 approached 0.5, indicating that the two fluids were mixed completely. In the straight microchannel, the green area gradually increased in the area where mixing of fluids 1 and 2 started. On the other hand, in the simulation of the helical micromixer, the mixing of the two fluids started as soon as they contacted each other as seen in the deformed shape due to the rotation (Figure 1c and Figure S1, Supporting Information). The green region in the helical channel was clearly larger than that at the same position for the straight channel. Figure 1d shows the relationship between the distance from the starting point of mixing and the mixing efficiency. The mixing efficiency M is defined as follows^[40–42]

$$\sigma = \sqrt{\frac{\sum (Y_n - \bar{Y})^2}{N}} \rightarrow M = 1 - \sqrt{\frac{\sigma^2}{\sigma_{\max}^2}} \quad (1)$$

where σ is the standard deviation of mass fraction, σ_{\max}^2 is the maximum variance of the mass fraction over the range interval, Y_n is the mass fraction at sampling point n , and \bar{Y} is the average mass fraction at the cross-section. As shown in Figure 1d, the efficiency of mixing in the helical microchannel increased with decreasing separation distance of grooves, and that having a 0.5 mm distance between the grooves was four times higher than that in the straight channel. The same improvement of the mixing was observed in fluids having viscosities from 0.99 mPa to 1.16 mPa s such as water or colored ink (Figure S2, Supporting Information). Volumetric flow rates from 0.2 to 1.0 mL min⁻¹ did not improve mixing efficiency much as shown in Figure S3 in the Supporting Information. Based on these results, we conducted the experiment using water and ink with flow rate of 0.3 mL min⁻¹.

In order to investigate the extent of the rotation as a function of the helical microchannel structure, the swirl number of the microchannels was adopted (Section S1 and Figure S4, Supporting Information). In the definition of the number, the numerator integrates axial and circumferential velocity, and the denominator integrates by squaring axial velocity. This equation indicates the degree of the rotation flow in channels. Figure S5 in the Supporting Information shows that the swirl number was almost constant regardless of the distance from

the starting point of mixing. As shown in Figure 1e, the swirl number of the microchannels decreased with respect to the distance between the grooves, indicating that the shorter distance between grooves improved the mixing efficiency by causing strong rotation of the fluids. The change of swirl number was large between a groove separation distance (GSD) of 0.5–2 mm. However, it gradually becomes smaller above 2 mm. As GSD is increased, the value approaches zero. For the 1.0 mm GSD, the mixing efficiency reached approximately 80% at 5 mm from the starting point of mixing. On the other hand, it reached 80% at 2 mm from the starting point for the 0.5 mm separation distance. Theoretically, the rotation flow might be promoted as long as there are grooves inside the channels. However, the promotion of the rotation flow depends on fabrication limitations. The T-shaped micromixer^[1] needs 8.64 mm from the starting point of mixing to reach approximately 80% at the almost same Reynolds number. Although it is difficult to compare our simulation with simulations in other studies, our helical micromixer sufficiently promotes the mixing efficiency.

In order to realize the desired helical microchannels having micrometer scale grooves, we used lost-wax casting with 3D-printed wax molds as shown in Figure 2a. Conventional lost-wax casting is a method which duplicates sculptures by melting a wax mold that is the same as the mold of the original sculpture. In this study, the wax mold of a 3D microchannel is embedded into a PDMS block. Then, the 3D microchannel can be formed inside PDMS blocks by removing the mold through heating to melt it. Compared with the conventional soft lithography method, this method can save steps in the fabrication process.

The 3D-printed microchannel mold was put on a cured PDMS block (Figure 2a-i), and liquid PDMS was added to embed it (Figure 2a-ii). This was cured at 40 °C. After curing, the device was set in an oven at 105 °C for 60 min to melt wax resin. Water was injected into the microchannels within 1 min after taking the hot device from the oven, and the wax was removed from the microchannels inside the PDMS block (Figure 2a-iii). Finally, the helical or straight microchannel was formed in the PDMS block (Figure 2a-iv,b–d). In this study, our helical micromixer required grooves inside the microchannels, which meant the printer needed around 10 μm resolution to control the mixing efficiency. To satisfy these design requirements, an inkjet-type 3D printer having excellent resolution was used. In addition, we selected the wax resin used according to the material of the microchannel mold. For microchannel fabrication using 3D-printed molds, ABS resin is often used as the mold.^[34] However, for fabrication using 3D-printed ABS molds, acetone must be injected into the microchannels to remove the mold. This causes swelling and damage of the microchannels. For 3D printing of soft wax based on an FDM method, the surface of the 3D-printed mold becomes bumpy.^[43] On the other hand, inkjet-type 3D printing of hard wax can realize smooth and fine structures (Figure S6, Supporting Information), so that our fabrication method can form grooves inside microchannels and avoid rough structure surfaces.

The fabrication accuracy of some microchannels is shown in Figure S7 in the Supporting Information. Figure S7a in the Supporting Information shows cross-sectional views of microchannels having 50, 100, 150, and 200 μm groove depths.

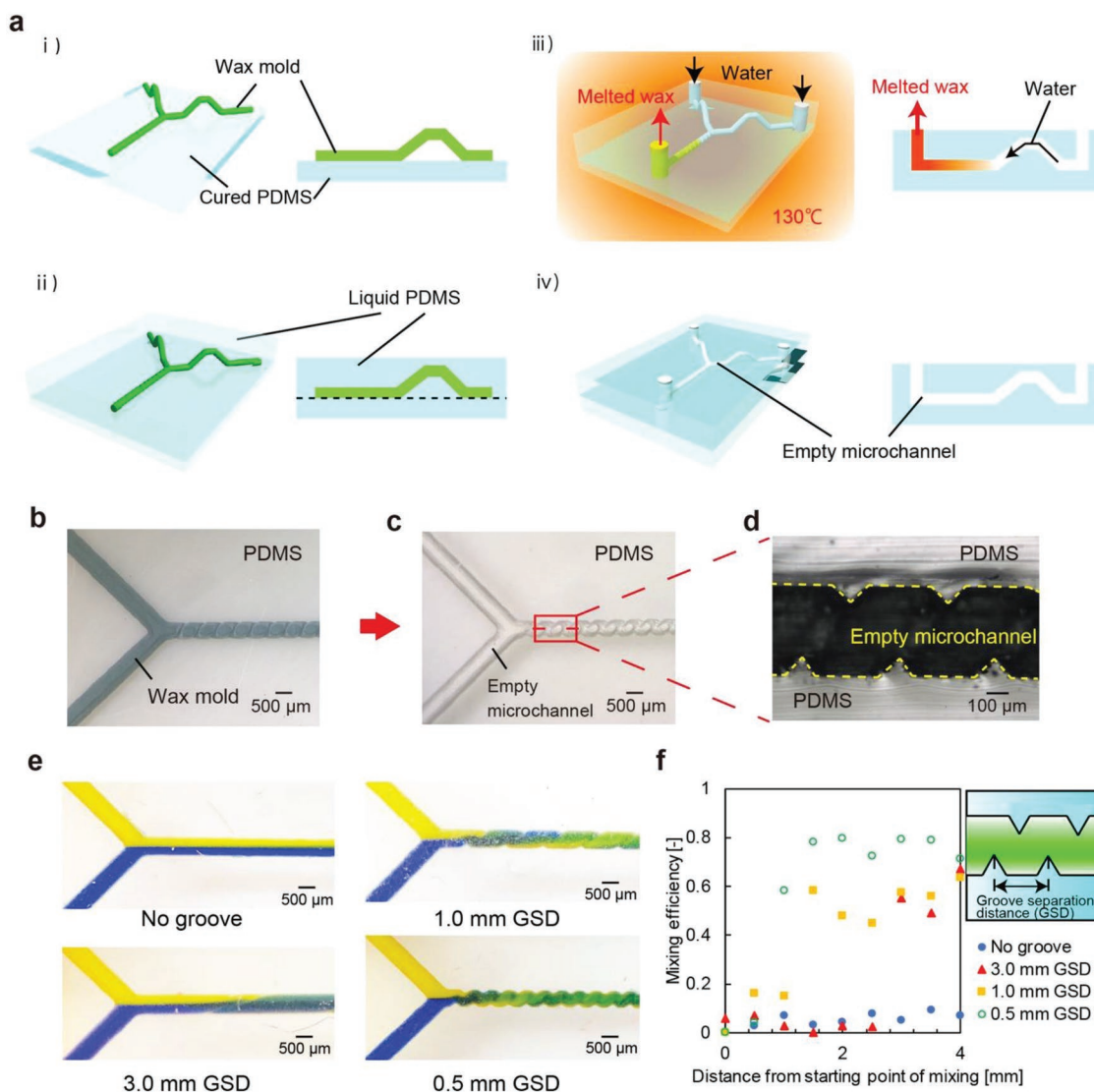


Figure 2. Fabrication by micro lost-wax casting and demonstration of the 3D helical micromixer. a) Microchannel fabrication process. b–d) Photographs of actual wax mold fabricated with a 3D printer. e) Photographs of fluids mixing in the straight (no groove) and helical microchannels having 3.0, 1.0, and 0.5 mm GSD. In the straight channel, yellow and blue fluids flow in parallel. For the 3D helical micromixer having 1.0 and 3.0 mm GSD, the green areas indicate mixing of yellow and blue fluids increases gradually with distance from the starting point of mixing. In the helical micromixer having 0.5 mm GSD, the green mixture appears as soon as yellow and blue fluids contact at the starting point of mixing. f) Mixing efficiency calculated from standard deviation of gray scale color on the cross-section with respect to distance from the starting point of mixing. Mixing efficiency becomes high with decreasing distance between the grooves.

However, the measured depths were around 30 μm less than the designed value as shown in Figure S7b in the Supporting Information. The reason for this difference might be the resolution of the 3D printer. The minimum thickness of one layer in the 3D printer was 13 μm . It might be difficult to realize sharp tips of triangular sloping grooves, since the tip area must be small. Therefore, the actual depth of the grooves was 30 μm lower than the desired value, and was equal to a two-layer thickness.

Figure 2e,f shows the results when mixing yellow and blue inks in the microchannels. In order to compare the efficiency of the mixing, a simple Y-shaped mixer was selected. Our method may have the potential for making more complicated

structures based on chaotic advection and parallel lamination in order to realize a higher efficiency of mixing. The green areas clearly indicated the amount of mixing of yellow and blue inks started increasing at a shorter distance for the microchannel with 0.5 mm groove separation. The mixing efficiency of yellow and blue inks increased with decreasing distance between grooves. In order to evaluate the mixing efficiency, we did experiments using water and red ink as shown in Figure S8 in the Supporting Information. Standard deviations of the complementary color (green) to red in the cross-sections were calculated from histograms of an 8-bit gray-scaled image converted from the image in which green was extracted. The reason why a complementary color was used was that red in the color image

becomes black in the gray-scaled image, since the white background included red, blue, and green elements. As shown in the results in Figure 2f, the distance at which mixing efficiency reached 60% was 3.0 mm from the starting point of mixing at the GSD of 3.0 mm, 1.5 mm at the GSD of 1.0 mm, and 1.0 mm at the GSD of 0.5 mm. The mixing efficiency at 4 mm from the starting point of mixing of the helical micromixer was more than eight times higher than for the straight-type micromixer. In addition, Figure S9 in the Supporting Information shows the calculated mixing efficiency results for various groove depths. The efficiency was the highest for the 133 μm GSD in the straight microchannel and in the helical micromixers having the 59 and 133 μm depth grooves. The relationship between swirl number and mixing efficiency is shown in Figure S10 in the Supporting Information. The swirl number was calculated as described in Section S1 in the Supporting Information. For both experimental and simulated results, the efficiency increased as a function of the swirl number, which verified our concept of the micromixer.

We fabricated the helical micromixer having a 3D bridge structure as one of the applications having a more complex structure made by the same method, and yellow and blue inks were injected as shown in Figure 3. Figure 3a shows the fabrication method of the microchannel. Schematics of the shape and mold used are Figure 3b,c and Figure S11 in the

Supporting Information. The yellow and blue inks were separated under the bridge structure of the straight microchannel (Figure 3d). On the other hand, in the helical microchannel (Figure 3e), the two fluids were mixed, and the fluid mixture was green in the microchannel before reaching the 3D bridge structure. Our lost-wax casting method required only one step to make the 3D microchannel. Furthermore, the microchannel mold was fabricated from a 3D printer directly. This leads to savings in micromixer fabrication time and cost. As shown in Figure S6 in the Supporting Information, the limit of wax modeling is a diameter of about 200 μm with a smooth surface. The actual resolution of channels with a smooth surface was better than the one using FDM methods^[31–34] and the direct printing of microchannel devices.^[25,44,45] Channels smaller than 200 μm can be printed by an inkjet type printer as the resolution of the printer itself is 13 μm . However, it was difficult to make a helical channel in the bridge structure parts. It is necessary to consider the design of molds according to the requirements of the channel and fabrication process. The resolution of microchannels and the flexibility of channel designs might be improved as a function of the development in 3D printer technology.

In conclusion, we proposed a micromixer with a helical structure made by lost-wax casting. Using CFD simulation, we modeled the helical micromixer to obtain the optimum design. The micromixer with 0.5 mm separation between grooves of

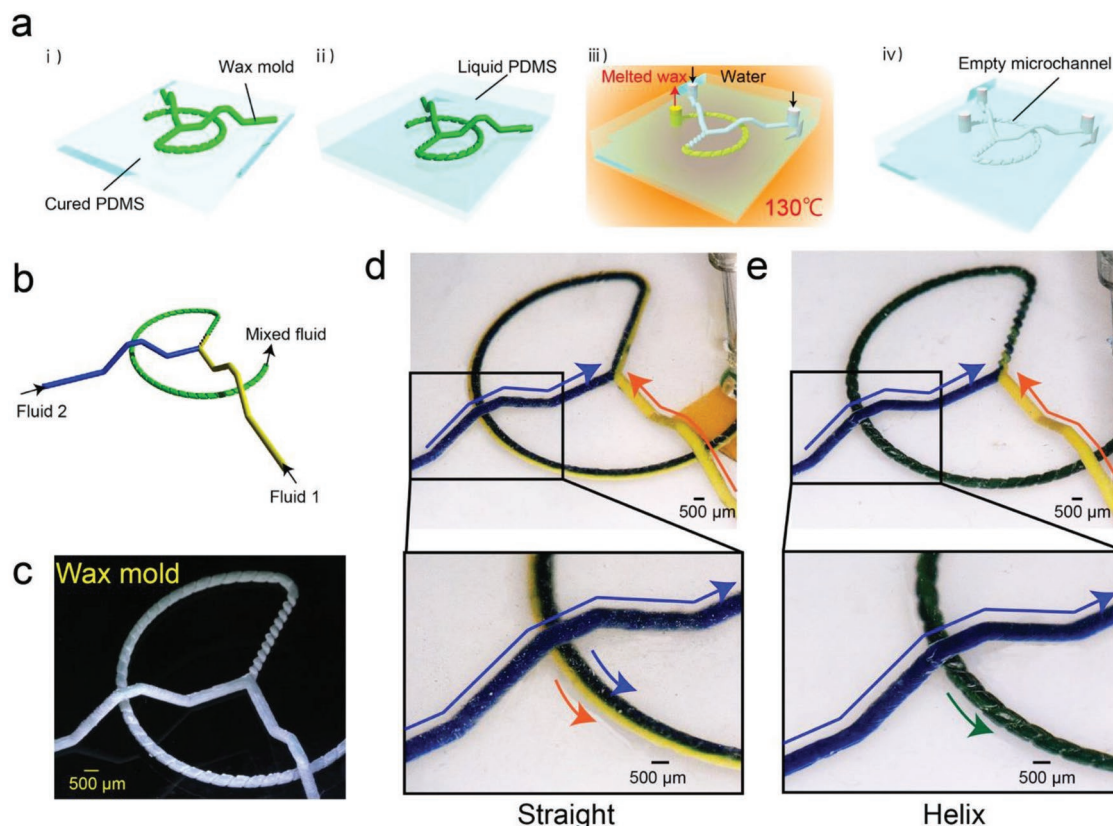


Figure 3. Monolithic microchannel composed of a helical micromixer and a 3D bridge structure. a) 3D microchannel fabrication process. b) Schematic of the microchannel. The microchannel is composed of two bridge structures and a helical micromixer. Two fluids are injected into the microchannels of the bridge structures, and the mixed fluid passes through them. c) The 3D-printed mold of the microchannel. d) Microchannel composed of a straight microchannel and bridge structures. e) Microchannel composed of a helical micromixer and bridge structures.

150 μm depth had approximately 80% mixing efficiency at a position 2 mm from the starting point of mixing of two fluids; this was improved compared to the mixing efficiency of other micromixers. The micro-scale lost-wax casting simplified the fabrication of 3D microchannels compared to conventional soft lithography fabrication. The proposed helical micromixer had more than eight times higher mixing efficiency than the straight-type micromixer. In addition, we demonstrated 3D printing-assisted microfabrication of the monolithic microchannel having the helical 3D structure. Through simulation and experiments, we showed device requirements for the architecture and fabrication characteristics. This work presents an important step toward the realization of micro-scale lost-wax casting and fabrication of 3D helical micromixers that offer low cost manufacturing and efficient POCT.

Experimental Section

CFD Analysis: In order to simulate mixing efficiency, CFD analysis (ANSYS Fluent, ANSYS Inc.) was performed based on computer aided design (CAD) data of the microchannel shape. In this simulation, the viscosities of the fluid which flowed inside the microchannels were assumed to be 1.003 and 0.99 mPa s considering water and ink used in this study. In order to observe characteristics of volumetric flow rate, fluid flow rate in the microchannels was assumed to be 0.3 mL min^{-1} . To measure the mixing rate at each position, the mass fractions of fluids on the cross-section were calculated at every 1 mm from the starting point of mixing. The standard deviation of the mass fraction of the cross-section was used as the degree of the mixing as described in the literature.^[40,41]

PDMS Microfluidic Chip Fabrication Method: In this study, the fabrication of 3D helical microchannels was based on micro-scale lost-wax casting as follows. First, a desired 3D microchannel mold of the micro helical structure was printed with a 3D printer (T76PLUS, Solidscape Co.). The printed microchannel mold was set onto a cured PDMS block. Liquid PDMS was additionally poured onto the printed molds of microchannel and this assembly was cured in a dry oven (VOS-301SD) at 40 °C for 24 h. The cured PDMS block including the wax microchannels was further heated at 130 °C for 1 h in the oven. Water at 25 °C was injected into the wax microchannels. The melted wax was flowed from the microchannels.

Experiment of Y-Shaped Helical Micromixer: Yellow and blue inks (STORIA, Sailor Pen Co.) were injected into two inlets each connected to a syringe pump (YSP-301 or Harvard Apparatus). In this study, the flow rate was 0.3 mL min^{-1} . In case of demonstration, blue and yellow inks were used as shown in Figure 2e. However, it was difficult to calculate the degree of the mixing in detail by blue and yellow inks. In order to measure the degree of mixing, water and the one which contained red ink were used in the experiments. The mixing efficiency was analyzed from the captured images by image analysis software (Image J) (Figure S8, Supporting Information). The green color in each pixel on the captured image was extracted from the RGB image. The green color image was converted to gray-scale image. In the gray-scale image, the red ink part showed as black. The black level on the straight line perpendicular to the flow at every 500 μm from the starting point of mixing was measured. The standard deviation of the gray level on the straight line was associated with the degree of the mixing of the red ink. That is, a small standard deviation indicated a high degree of mixing, and vice versa.

Supporting Information

Supporting Information is available from the Wiley Online Library or from the author.

Acknowledgements

This work was supported by the Japan Science and Technology Agency, PRESTO Grant Number JPMJPR18J2; a Takeda Science Foundation Grant; and a Life Science Research Grant, and MIC/SCOPE Grant Number 181603007. H.O. acknowledges support from a Grant-in-Aid for Young Scientists (A) and Grant-in-Aid for Challenging Exploratory Research provided by the Japan Society for the Promotion of Science.

Conflict of Interest

The authors declare no conflict of interest.

Keywords

3D printers, lost-wax casting, micromixers

Received: September 9, 2019

Revised: October 25, 2019

Published online:

- [1] X. Chen, T. Li, H. Zeng, Z. Hu, B. Fu, *Int. J. Heat Mass Transfer* **2016**, *98*, 131.
- [2] P. Garstecki, M. J. Fuerstman, M. A. Fischbach, S. K. Sia, G. M. Whitesides, *Lab Chip* **2006**, *6*, 207.
- [3] Q. Zhou, A. Sussman, J. Chang, J. Dong, A. Zettl, *Sens. Actuators, A* **2015**, *223*, 67.
- [4] U. Khan, T. H. Kim, K. H. Lee, J. H. Lee, H. J. Yoon, R. Bhatia, I. Sameera, W. Seung, H. Ryu, C. Falconi, S. W. Kim, *Nano Energy* **2015**, *17*, 356.
- [5] A. A. S. Bhagat, H. Bow, H. W. Hou, S. J. Tan, J. Han, C. T. Lim, *Med. Biol. Eng. Comput.* **2010**, *48*, 999.
- [6] A. A. S. Bhagat, H. W. Hou, L. D. Li, C. T. Lim, J. Han, *Lab Chip* **2011**, *11*, 1870.
- [7] M. E. Warkiani, A. K. P. Tay, B. L. Khoo, X. Xiaofeng, J. Han, C. T. Lim, *Lab Chip* **2015**, *15*, 1101.
- [8] N. Misawa, H. Mitsuno, R. Kanzaki, S. Takeuchi, *Proc. Natl. Acad. Sci. U. S. A.* **2010**, *107*, 15340.
- [9] S. J. Tan, L. Yobas, G. Y. H. Lee, C. N. Ong, C. T. Lim, *Biomed. Microdevices* **2009**, *11*, 883.
- [10] P. Yager, T. Edwards, E. Fu, K. Helton, K. Nelson, M. R. Tam, B. H. Weigl, *Nature* **2006**, *442*, 412.
- [11] Y. Kasai, S. Sakuma, F. Arai, in *MHS 2017 – 28th 2017 Int. Symp. Micro-NanoMechatronics and Human Science* (Eds: S. Hata, J. Sakurai, M. Mizoshiri), IEEE, Piscataway, NJ **2018**, p. 1.
- [12] W. Ehrfeld, K. Golbig, V. Hessel, H. Löwe, T. Richter, *Ind. Eng. Chem. Res.* **1999**, *38*, 1075.
- [13] Y. K. Suh, S. Kang, *Micromachines* **2010**, *1*, 82.
- [14] H. Aref, J. R. Blake, M. Budišić, S. S. S. Cardoso, J. H. E. Cartwright, H. J. H. Clercx, K. El Omari, U. Feudel, R. Golestanian, E. Guillard, G. F. Van Heijst, T. S. Krasnopolskaya, Y. Le Guer, R. S. MacKay, V. V. Meleshko, G. Metcalfe, I. Mezić, A. P. S. De Moura, O. Piro, M. F. M. Speetjens, R. Sturman, J. L. Thiffeault, I. Tuval, *Rev. Mod. Phys.* **2017**, *89*, 025007.
- [15] X. Mao, B. K. Juluri, M. I. Lapsley, Z. S. Stratton, T. J. Huang, *Microfluid. Nanofluid.* **2010**, *8*, 139.
- [16] J. H. Tsai, L. Lin, *Sens. Actuators, A* **2002**, *97–98*, 665.
- [17] K. Iwai, K. C. Shih, X. Lin, T. A. Brubaker, R. D. Sochol, L. Lin, *Lab Chip* **2014**, *14*, 3790.
- [18] P. J. Lee, P. J. Hung, V. M. Rao, L. P. Lee, *Biotechnol. Bioeng.* **2006**, *94*, 5.

- [19] J. Li, M. Wu, J. Chu, R. Sochol, S. Patel, *Biochem. Biophys. Res. Commun.* **2014**, *444*, 562.
- [20] Y. Morimoto, M. Kato-Negishi, H. Onoe, S. Takeuchi, *Biomaterials* **2013**, *34*, 9413.
- [21] Y. Xia, G. M. Whitesides, *Annu. Rev. Mater. Sci.* **1998**, *28*, 153.
- [22] L. Lin, Y. T. Cheng, K. Najafi, K. D. Wise, USA, *Patent No. US 6232150 B1*, **2001**.
- [23] N. Sundararajan, M. S. Pio, L. P. Lee, A. A. Berlin, *J. Microelectromech. Syst.* **2004**, *13*, 559.
- [24] C. S. Chen, D. N. Breslauer, J. I. Luna, A. Grimes, W. C. Chin, L. P. Lee, M. Khine, *Lab Chip* **2008**, *8*, 622.
- [25] H. Ilkhani, H. Zhang, A. Zhou, *Sens. Actuators, B* **2019**, *282*, 675.
- [26] S. Y. Wu, C. Yang, W. Hsu, L. Lin, *Microsyst. Nanoeng.* **2015**, *1*, 1.
- [27] S. Maruo, J. T. Fourkas, *Laser Photonics Rev.* **2008**, *2*, 100.
- [28] R. A. Farrer, C. N. LaFratta, L. Li, J. Praino, M. J. Naughton, B. E. A. Saleh, M. C. Teich, J. T. Fourkas, *J. Am. Chem. Soc.* **2006**, *128*, 1796.
- [29] J. T. Fourkas, C. N. LaFratta, USA, *Patent No. US 9656414 B2*, **2017**.
- [30] R. D. Sochol, E. Sweet, C. C. Glick, S. Y. Wu, C. Yang, M. Restaino, L. Lin, *Microelectron. Eng.* **2018**, *189*, 52.
- [31] W. H. Goh, M. Hashimoto, *Macromol. Mater. Eng.* **2018**, *303*, 1700484.
- [32] W. H. Goh, M. Hashimoto, *Micromachines* **2018**, *9*, 523.
- [33] W. Tang, H. Liu, L. Zhu, J. Shi, Z. Li, N. Xiang, J. Yang, *Micromachines* **2019**, *10*, 544.
- [34] V. Saggiomo, A. H. Velders, *Adv. Sci.* **2015**, *2*, 1500125.
- [35] C. Shan, F. Chen, Q. Yang, Z. Jiang, X. Hou, *Micromachines* **2018**, *9*, 29.
- [36] A. Koh, D. Kang, Y. Xue, S. Lee, R. M. Pielak, J. Kim, T. Hwang, S. Min, A. Banks, P. Bastien, M. C. Manco, L. Wang, K. R. Ammann, K. I. Jang, P. Won, S. Han, R. Ghaffari, U. Paik, M. J. Slepian, G. Balooch, Y. Huang, J. A. Rogers, *Sci. Transl. Med.* **2016**, *8*, 366ra165.
- [37] J. B. Chossat, Y. Tao, V. Duchaine, Y. L. Park, in *Proc. – IEEE Int. Conf. Robotics and Automation* (Eds: G. Antonelli, D. Burschka, I. M. Chen, N. Y. Chong, V. Krovi, D(Dongheui). Lee, D(Dongjun). Lee, Y. Li, P. Martinet, J. Neira, P. Oh, N. Simaan, Y. Sun, K. Sycara, K. Yokoi), IEEE, Piscataway, NJ **2015**, p. 2568.
- [38] M. Bariya, H. Y. Y. Nyein, A. Javey, *Nat. Electron.* **2018**, *1*, 160.
- [39] A. Koivikko, V. Sariola, in *RoboSoft 2019 – 2019 IEEE Int. Conf. Soft Robotics*, IEEE, Piscataway, NJ **2019**, p. 509.
- [40] W. Raza, S. Hossain, K. Y. Kim, *Sens. Actuators, B* **2018**, *258*, 381.
- [41] H. S. Santana, D. S. Tortola, J. L. Silva, O. P. Taranto, *Energy Convers. Manage.* **2017**, *141*, 28.
- [42] X. Chen, T. Li, *Chem. Eng. J.* **2017**, *313*, 1406.
- [43] Z. Li, J. Yang, K. Li, L. Zhu, W. Tang, *RSC Adv.* **2017**, *7*, 3313.
- [44] P. J. Kitson, M. H. Rosnes, V. Sans, V. Dragone, L. Cronin, *Lab Chip* **2012**, *12*, 3267.
- [45] A. K. Au, W. Lee, A. Folch, *Lab Chip* **2014**, *14*, 1294.